Experimental investigation of the shear dynamic behavior of double-lap adhesively bonded joints on a wide range of strain rates

Georges Challita, Ramzi Othman, Pascal Casari, Khaled Khalil

Experimental investigation of the shear dynamic behavior of double-lap adhesively bonded joints on a wide range of strain rates

Georges Challita [a,b], Ramzi Othman [a], Pascal Casari [a], Khaled Khalil [c]

[a] Institut de Recherche en Génie Civil et Mécanique, Ecole Centrale de Nantes et, Université de Nantes, 1 Rue de la Noë BP 92101, F-44321 Nantes cedex 3, France
[b] Département de Mécanique, Équipe Mécanique des Milieux Complexes (MMC), Faculté de Génie Branche 2, Université Libanaise, Roumieh, Lebanon
[c] Département de Mécanique, Faculté de Génie Branche 1, Université Libanaise, Tripoli, Lebanon

The main concern of this work is the mechanical characterization of adhesively bonded assemblies under dynamic shear loading ranging from quasi-static (10^{-4} s^{-1}) up to high (10^{4} s^{-1}) strain rates. The double-lap shear sample is proposed and a bonding procedure is established. The assemblies are made of steel substrates bonded with an epoxy adhesive. Two surface treatments of the substrates are considered: ethanol and sand shooting. The shear strength and the failure strain are measured by taking into account the testing setups accuracy and the non-uniform distribution of the stress and strain fields in the overlap region. The sensitivity of the strength and the failure strain to the strain rate is highlighted; it is found that the failure strain decreases and the shear strength increases with the strain rate until reaching a maximum value then it drops for very high strain rates.

Keywords:
Lap shear
Stress distribution
Impact
Strain rate
Hopkinson bar
Surface treatment

1. Introduction

For several decades, adhesively bonded assemblies have gained an increasing interest in the industry. Due to many advantages such as simplicity, lightness and low cost, bonding has been used as an assembling technique between many substrates. The most widespread loading case is static shear, but these assemblies may undergo dynamic loading such as shock or impact depending on their practical applications. Studying the dynamic behavior of these assemblies is becoming nowadays a real challenge, especially if we consider the high number of factors that influence such structures.

Several publications have studied the experimental characterization of bonded assemblies under dynamic loading. Because of a lack of standards, many specimen geometries were proposed and several setups were used. Zachary and Burger [1] and Rossamanith and Shukla [2] investigated the stress field in single-lap joints using dynamic photo-elasticity. Beevers and Ellis [3] used a special drop-weight tower to assess the impact response of a single-lap adhesive joint; the yield strength of the substrate was strain rate-dependent which influenced the results. A special drop testing device was designed in Ref. [4]. This setup was used to compare bonded assemblies, pop-riveted assemblies and spot-welded assemblies under combined tension and shear loading. Bezemer et al. [5] used a rod-and-ring specimen impacted by a drop-weight system and a compressive air gun to test the shear failure energy in bonded joints.

Alternatively to the drop-weight technique, the impact pendulum technique have been applied to characterize bonded assemblies. Harris and Adams [6] used this last technique to examine the crashworthiness of bonded structures in vehicles manufacturing. They also applied the block impact technique to a single-lap joint to evaluate the joint strength [7]. The impact pendulum technique is also applied to assess collision safety of bonded assemblies with dissimilar metallic substrates for automotive applications [8]. Recently, Goglio and Rossetto [9] used an instrumented impact pendulum setup to test adhesively single-lap joint with substrates of a classical dog-bone geometry under different peel and shear ratios.

The drop-weight and the impact pendulum techniques are, however, limited with the maximum reached velocity [5]. For high impact speeds (> 5 m/s), one of the most accurate and simplest methods is the split Hopkinson pressure bar (SHPB) which is in continuous increasing use in the recent years due to its high reliability and easy manipulation. Keisler and Lataillade [10] were the first to apply this technique to bonded assemblies. They mainly examined the effects of substrates surface roughness and wettability. Yokoyama [11] proposed a pin-and-collar specimen geometry to measure the shear strength of bonded joints. Alternatively, a single-lap, double-L shaped specimen is used in Ref. [12]. Recently, this geometry is used to assess the influence of temperature and strain rate on the joint shear strength [13]. However, this double-L geometry does not ensure constant impedance. In the case of the split Hopkinson bar setup, the incident wave will reflect before arriving to the adhesive joint because of the change in impedance. This induces inaccuracies in conventional Hopkinson bar analyses. To overcome this problem, Challita et al. [14,15] proposed the use of a double-lap sample. This geometry is also preferred to the

pin-and-collar [11] and rod-and-ring geometries [5], as it minimizes the peel stress. Recently, a tensile Hopkinson bar setup was used to assess temperature and velocity effects on strength for single-lap shear specimen [17].

In addition to the shear strength, the split Hopkinson bar technique was also used to investigate the response under tensile [16,18] and combined tension-torsion [20] loads. Lawrence-Wu et al. [19] also used this method to measure the energy absorption of electronic adhesives.

Recently, Challita and Othman [21] studied the accuracy of the split Hopkinson bar tests on double-lap bonded joints. They found that the conventional Hopkinson bar analysis correctly estimates the average stress in the joint. However, it overestimates the average strain as it considers that only the joints but not the substrates deform during the test. Moreover, it is showed that the maximum stress and strain in the joints cannot be estimated. Therefore, Challita and Othman [21] proposed numerically determined coefficients to obtain the correct average and maximum strains and the maximum stress in the specimen. We should notice that problems stated in Ref. [21] are not characteristics neither of double-lap geometry nor the Hopkinson bar setup. These problems are rather depending on the adhesively bonded-joints geometry.

In this paper, we show results obtained from a wide experimental program aiming at characterizing the shear behavior of bonded assemblies on an important range of strain rates. The assemblies were made of steel substrates, bonded with an epoxy adhesive film. Three different setups were applied for this program: a screw-driven quasi-static machine, a servo-hydraulic machine and a Hopkinson bar system. Two configurations of the servo-hydraulic machine and Hopkinson bar technique were used. The modified servo-hydraulic machine presented in Ref. [22] is used for the upper intermediate strain rate range, whereas the direct-impact Hopkinson bar method is used for the very high strain rates. In order to obtain accurate stress and strain measurements, the numerically determined coefficients proposed in Ref. [21] were applied to correct the stress and the strain calculated from force and displacements measurements recorded at the substrates boundaries. The paper contains three sections along with an Introduction (Section 1) and a Conclusion (Section 6). Section 2 provides a description of the experimental program and the corresponding methodology. Subsequently, Section 3 presents results obtained from the different mechanical testing setups. A discussion, which highlights the most interesting findings, is given in Section 5.

2. Method

2.1. Materials

The considered bonded assemblies are made from steel S235 substrates. Their Young's modulus, Poisson's ratio and density are equal to 200 GPa, 0.3 and 7800 kg/m^3, respectively. The adhesive is a toughened epoxy adhesive film SA 80 distributed by GURIT. Its Young's modulus, Poisson's ratio and density are equal to 3 GPa, 0.4 and 1230 kg/m^3, respectively. This adhesive is a toughened epoxy film on a glass carrier available for bonding of composite skins to cores, or metal substrates on any metal or laminated composite material. It provides high strain to failure and high toughness.

2.2. Sample geometry

A double-lap geometry, named also M-shape geometry, was chosen for dynamic shear testing at different strain rate ranges as proposed in Refs. [14,15]. This geometry has many advantages:

- It does not impose any modifications on the testing setups to mount the specimen (slits, hollows, additional fixtures,...).
- The impedance mismatch brought by this geometry does not create many wave reflections and thus the quality of the recorded signals at high strain rates is quite good.
- The quite simple geometry facilitates the experiment preparation, reduces potential errors and saves time.

Two kinds of double-lap specimens were used. The first, named *compression-shear* specimen, transforms the compressive load applied by the testing machine to a shear load in the adhesive joint, whereas the second kind of specimen converts the testing machine tensile load to a shear load in the joint.

2.2.1. Compression-shear specimen

The conventional mechanical frame and the SHPB setup can easily deliver a compressive load. In order to get a shear stress state in the bonded joint, the specimen geometry should be designed in a way to transform the initial compressive load (imposed on the substrates) to a shear load on the joint. The compression-shear sample presented in Fig. 1 fulfills this requirement. Such sample geometry has the advantage that there is no need for grips. However, friction may have some effects, especially if sliding occurs at the edges between the machine and the specimen. Fortunately, they can be reduced by the use of lubricant. The compression-shear specimen consists in three rectangular plates of the same length and width bonded together. The upper and lower plates are identical and parallel. The middle plate is shifted by 2 mm from the two others in the length direction; this gap allows the conversion from compression load on the specimen to shear stress inside the adhesive layer. In this paper, the three plates are 12-mm wide. The extreme plates are 2-mm thick while the central one is 4 mm thick. All specimens were prepared with the mounting device which will be presented below. Three overlap lengths were considered: 10, 12 and 14 mm imposing the substrate lengths to 12, 14 and 16 mm, respectively.

2.2.2. Tensile-shear specimen

Servo-hydraulic machines can provide compression and tensile loads. However, a damping system is needed for compression testing at high velocities. It is, therefore, preferred to use the tensile loading configuration. For servo-hydraulic machine, the adopted geometry should convert this tensile load to a shear stress state in the adhesive. In this case, clamping must be ensured and leads to use another kind of substrates shape named tensile-shear specimen. Then, each of the three substrates is ended with a half dog-bone shape [9] with dimensions shown in Fig. 2. Holes are machined out to allow screwing the specimen to the clamping device of the crossheads of the apparatus. The substrate thicknesses had the same values as the compression-shear specimens one. In this case, an overlap length of 14 mm was chosen.

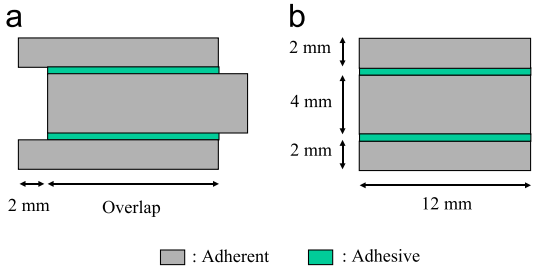

Fig. 1. Compression-shear sample: (a) longitudinal view and (b) transverse view.

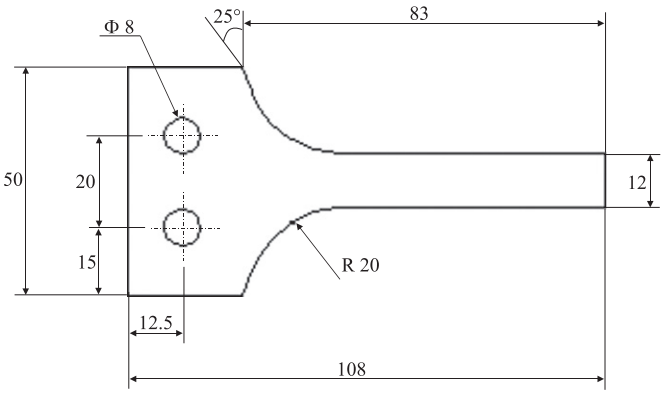

Fig. 2. Adherent geometry of the tension-shear specimen.

2.3. Bonding procedure

In order to ensure the repeatability, the same bonding procedure was followed in the preparation of both kinds of specimens. The bonding procedure is divided in the following steps:

1. All three substrate plates are sanded with glass paper P220.
2. The substrates are then wiped with dry paper.
3. Five points on determined positions are marked on each plate where thicknesses are measured using a micrometer; an average value is thereafter calculated.
4. The mounting device is cleaned with ethanol and coated with a release agent to avoid adhesion between the specimen and the mounting through the overflowed adhesive.
5. The surfaces to be bonded are cleaned three times with ethanol and the paper is changed each time. In addition, for about one half of the samples, the substrate surfaces are shot with pressurized sand under 3 bars for 7–8 s. The distance between the surface and the gun is 5–6 cm. Subsequently, a compressed dry air is used to remove sand particles off the surface which is finally cleaned with acetone.
6. The surface roughness of each substrate is measured (average distance between higher and lower peaks). The average roughness in case of ethanol treatment is $R_a = 1.4$ μm and for sand shooting treatment $R_a = 2.0$ μm.
7. The epoxy film is cut into pieces with dimensions matching the adhesive joint surfaces. The total film weight is 175 g/m^2, with a glass carrier of 25 g/m^2.
8. The three substrates are adjusted with the lateral screws to the mounting device presented in Fig. 3, and the whole assembly is put under uniform pressure by a vertical screw and a spring.
9. The overall assembly is put in an oven where the cure cycle of the adhesive is programmed with respect to the data sheet of the SA 80 film. The cure cycle consists in a temperature ramp from the ambient till 120 °C at a rate of 2 °C/min and then the temperature is maintained constant for 45 min and finally a linear decrease down to room temperature.
10. After the end of the cure cycle, the specimen is removed from the mounting, the total thickness of the specimen is measured with the micrometer at the same five points marked initially on the substrates, and an average value is calculated. The adhesive joint thickness is the half difference between the total average thickness of the bonded assembly and the sum of the average thicknesses of the three substrates. The adhesive thickness is found to be 120 ± 15 μm.
11. Specimen are kept in a conditioned room (local temperature 20 °C, relative hygrometry 50%) for two to four weeks and tested within 2 h after leaving the conditioned room.

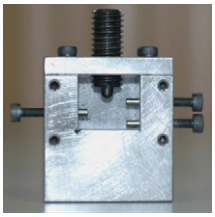

Fig. 3. Mounting device for compression-shear specimens.

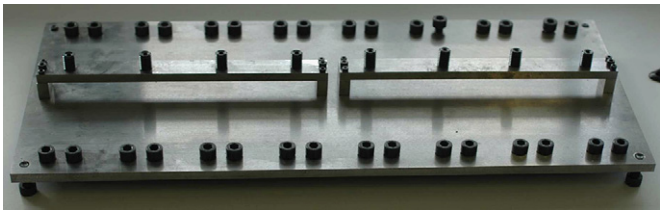

Fig. 4. Mounting device for tensile-shear specimens.

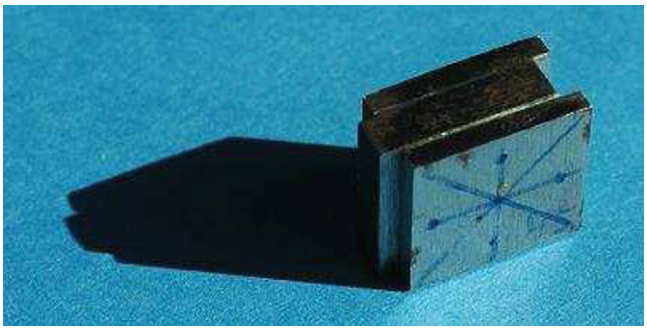

Fig. 5. Example of a compression-shear specimen.

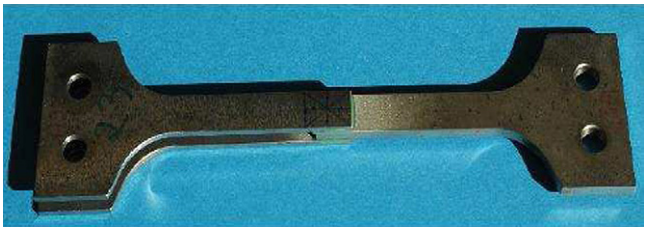

Fig. 6. Example of a tensile-shear specimen.

The same procedure was followed to prepare the tension-shear specimens excepting the mounting device. The mounting device for tensile specimens is shown in Fig. 4. We also show, in Figs. 5 and 6, photos for compression-shear and tension-shear specimens, respectively.

2.4. Experimental techniques

2.4.1. Quasi-static strain rates

The device used for these tests is a conventional quasi-static electro-mechanical computer controlled INSTRON 5584 machine. The specimen is placed on a stiff metallic grip connected to the base frame of the machine while the upper grip is mounted on a mobile crosshead. The load cell capacity of the machine is 150 kN ($\pm 0.2\%$ of inaccuracy) while the maximum displacement range and the speed of the crosshead are 1 m and 750 mm/min, respectively. Two testing speeds were considered: 0.1 and 10 mm/min.

With this quasi-static machine, the compression-shear samples were tested. The three overlap lengths were considered, i.e., 10, 12 and 14 mm.

2.4.2. Intermediate strain rates

A MTS 819 servo-hydraulic machine is used for tests at intermediate strain rates. The classical configuration of this setup, using a piezoelectric load cell, is applied for experiments at the two low velocities: 0.1 and 0.5 m/s. To avoid oscillations on the force measurement at high velocities a modified configuration of the servo-hydraulic machine, developed in Ref. [22], is applied for tests at 1 and 3 m/s. In its classical configuration, the MTS 819 machine consists in an upper stationary crosshead, where a piezoelectric force sensor (capacity of 25 KN) is mounted. This machine is equipped with a mobile lower crosshead controlled by a servo-hydraulic controlled jack. A LVDT type 205 integrated to the mobile jack measures the displacement history. The maximum speed reached with this setup is 16 m/s. The modified configuration uses a Hopkinson bar-like force sensor. The used bar is made of Marval steel. It is 820 mm long and 16 mm in diameter. Moreover, the redundant measurement wave separation technique [23–26] is used to overcome limitation on the test duration. For both the classical and modified configuration, the tensile-shear samples were used.

2.4.3. High strain rates

For high strain rate tests, the Hopkinson bar method was used. Two configurations were considered: the conventional two-bar configuration [27,28] and the direct-impact Hopkinson bar [29,30]. The conventional configuration of the Hopkinson bar technique consists of two MARVAL steel bars. The striker bar is made of the same material and has the same diameter as both incident and transmitted bars. The specimen comes in between the input and the output bars. Two strain gauge stations are bonded on the input and output bars, one on each bar. The input gauge station measures the incident and reflected waves and the output gauge records the transmitted wave. The two gauge signals are stored with a sampling rate of 10 MHz. Subsequently, we apply a 500 kHz low-pass numerical filter to the strain gauge signals which yields much lower noise levels. The signals are treated using DAVID software [31] to measure the forces and velocities at the specimen–bar interfaces. In order to shift the incident, reflected and transmitted waves, from the gauge stations where they are recorded, till the specimen–bar interfaces, the wave dispersion relation of the two bars is needed. This dispersion relation is measured by the method developed in Ref. [32]. With this technique the wave velocity is related to resonance positions observed through strain measurement on a long duration and wave damping is related to the bandwidth of these resonances. We should notice that the conventional Hopkinson bar configuration was used for striker impact velocities of 8 and 14 m/s. At a very high impact speed (> 20 m/s), it is suitable to apply the direct-impact technique in order to protect the strain gauge connections. Indeed, the striker impact induces not only a compressive longitudinal wave but also a transverse expanding wave. The amplitude of both waves increases with the impact velocity and for high velocities the amplitude of the transverse wave is high enough to break connections of the input bar strain gauge station. In the direct-impact configuration, the input bar is removed. The specimen is just maintained to the first end of the output bar by means of a special thin adhesive paper.

2.5. Measurement analysis

With the different experimental setups described above, we can measure the force and the displacement(s) (or velocity(ies)) at the substrates boundaries. From these measurements we aim at determining the average and the maximum strain and stress in the adhesive joint.

Let $F(t)$ be the force:

- measured by the piezoelectric load cell in the case of the quasi-static machine and the conventional configuration of the servo-hydraulic machine;
- determined by the BCGO wave separation technique in the case of the modified servo-hydraulic machine as detailed in Ref. [22];
- calculated by the transmitted wave recorded on the output bar in the case of the classical and direct-impact Hopkinson bar setup.

Assuming that this force applied to the substrate boundaries is exactly the same as the force applied to the adhesive joint, the stress in the adhesive can be approximated by

$$\sigma_{meas}(t) = \frac{F(t)}{2 \times l_0 \times w}, \tag{1}$$

where l^0 and w are the overlap length and the joint width, respectively. Challita and Othman [21] showed, by using finite

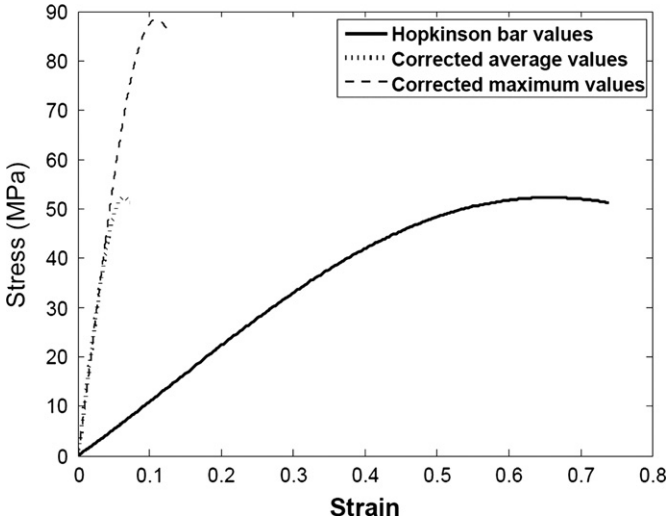

Fig. 7. Typical stress and strain corrections.

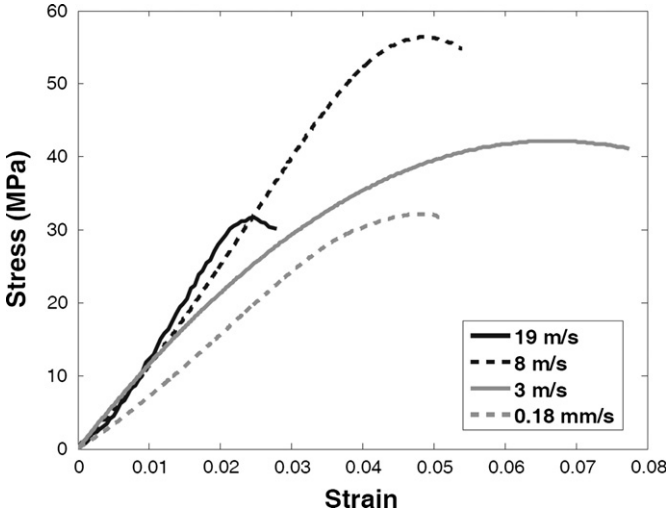

Fig. 8. Typical maximum stress–maximum strain curves obtained at different velocities.

element analysis, that the measured stress σ_{meas} estimates, with good accuracy, the average stress in the joint σ_{avg}, i.e.,

$$\sigma_{avg}(t) \approx \sigma_{meas}(t). \tag{2}$$

As the fracture is a main concern in adhesively bonded assemblies, Challita and Othman [21] proposed to determine the maximum stress in the joint, σ_{max}, by using a correcting coefficient:

$$\sigma_{max}(t) \approx \frac{\sigma_{avg}(t)}{\chi_\sigma} \approx \frac{\sigma_{meas}(t)}{\chi_\sigma}. \tag{3}$$

χ_σ is a constant which depends on the material and geometrical properties of the assembly and is numerically estimated. In the case of conventional Hopkinson bar setup, the values of this constant are taken from Ref. [21]. For the other setups, similar numerical simulations were carried out to identify the values of the coefficient.

Similarly, let $U_1(t)$ be the displacement of the central substrate end and $U_2(t)$ be the displacement of the upper and lower substrate ends. In the case of the quasi-static machine and the classical servo-hydraulic machine, the ends of the upper and lower substrates are clamped. Therefore, $U_2(t)=0$. The displacement of the central substrate end is measured by an LVDT sensor.

The displacement $U_1(t)$ is measured with same sensor in the case of the modified servo-hydraulic machine and $U_2(t)$ is calculated by the BCGO wave separation technique. This displacement is calculated from the transmitted wave in the two configurations of the Hopkinson bar method. In the case of the classical bar setup, $U_1(t)$ is computed knowing the incident and reflected waves in the input bar; while, in the case of direct-impact setup, this displacement is determined from the transmitted wave and the striker velocity. Consequently, we can obtain $U_1(t)$ and $U_2(t)$ in the case of different setups used. Assuming that the substrates are rigid, the shear strain in the joint can be approximated by

$$\varepsilon_{meas}(t) = \frac{U_2(t) - U_1(t)}{h_0}, \tag{4}$$

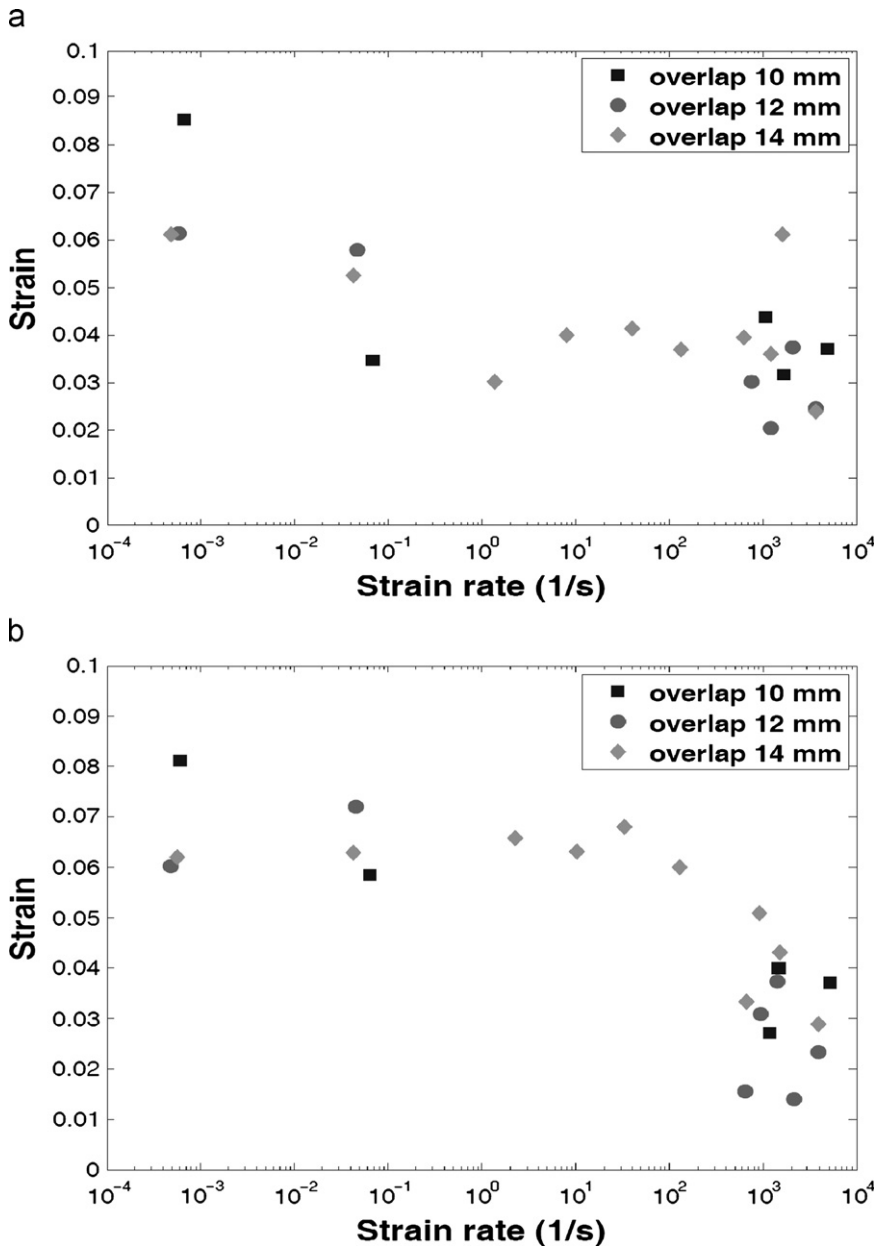

Fig. 9. Adhesive joint failure strain for adherents surface treatment with (a) ethanol and (b) sand shooting.

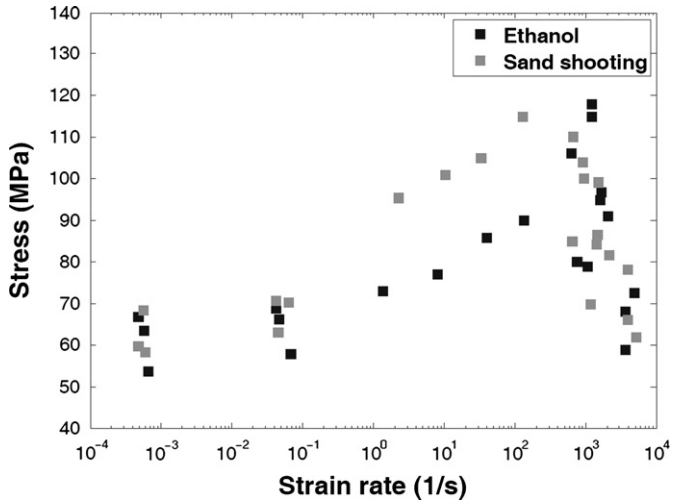

Fig. 10. Comparison between ethanol and sand shooting effects on the adhesive joint failure strain.

where h_0 is the thickness of the adhesive layer. Challita and Othman [21] showed that the measured strain ε_{meas} overestimates the average strain in the joint ε_{avg}, because it neglects the deformation of the substrates. They propose to write

$$\varepsilon_{avg}(t) \approx \beta_\varepsilon \varepsilon_{meas}(t), \tag{5}$$

and for the maximum strain ε_{max}:

$$\varepsilon_{max}(t) \approx \frac{\varepsilon_{avg}(t)}{\chi_\varepsilon} \approx \frac{\beta_\varepsilon \varepsilon_{meas}(t)}{\chi_\varepsilon}, \tag{6}$$

where β_ε and χ_ε are correcting constants determined numerically which depend on the material and geometrical properties of the assembly. As for χ_σ the values of β_ε and χ_ε are taken from Ref. [21] in the case of conventional Hopkinson bar setup. For the other setups, similar numerical simulations were carried out to determine the values of the two coefficients. It is worth noticing that the coefficients χ_σ,β_ε and χ_ε are calculated while assuming an elastic behavior of the adhesive. This is motivated by the brittle behavior of the adhesive as will be shown later in Fig. 8. Therefore, the post-elastic behavior can be neglected.

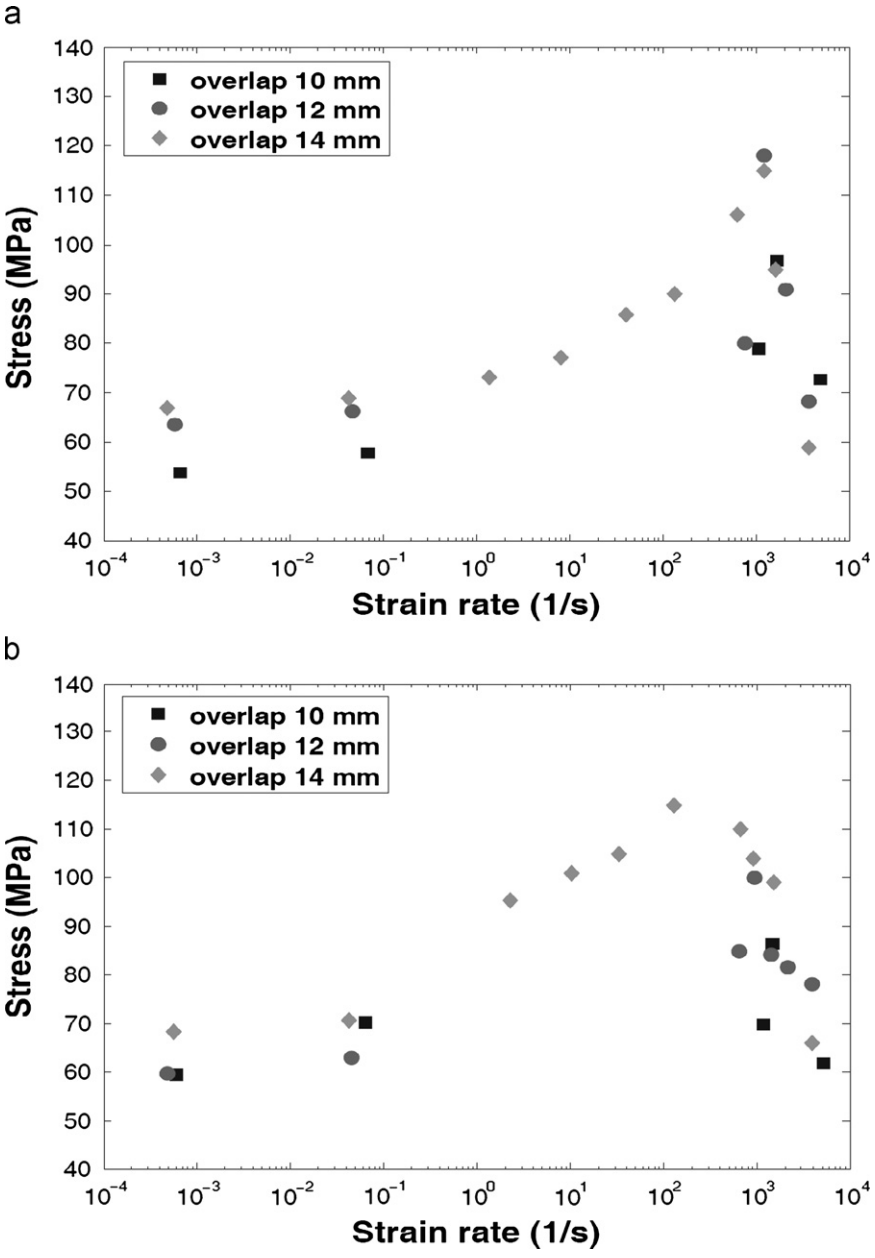

Fig. 11. Adhesive joint shear strength for adherents surface treatment with (a) ethanol and (b) sand shooting.

3. Results

3.1. Typical processing

In Fig. 7, a typical result, obtained with the conventional configuration of the Kolsky–Hopkinson setup, is presented. The black line represents the uncorrected stress–strain relation as obtained by Eqs. (1) and (4). Subsequently, the average stress–average strain relation (gray dotted line) is calculated by using Eqs. (2) and (5). Precisely, the strain is corrected by the constant β_ε. In the case of Fig. 7, $\beta_\varepsilon = 0.0983$. Then, Eqs. (3) and (6) are applied to deduce the maximum stress and maximum strain, respectively. $\chi_\varepsilon = \chi_\sigma = 0.592$ in the case of Fig. 7, where the maximum stress–maximum strain relation is represented with the gray dashed line. The failure shear stress is defined as the maximum of this curve and the failure shear strain is the strain at the failure at the failure stress. Fig. 7 shows clearly how important is the effect of corrections. An example of the maximun stress–maximum strain relations obtained at different velocities is given in Fig. 8. It comes that the joint behavior is highly strain rate sensitive.

3.2. Failure shear strain

For each test configuration (overlap length, surface treatment, strain rate), three tests are carried out, an average value of the shear strength and the failure strain is then calculated. In Figs. 9(a) and (b), the failure strain, obtained with ethanol and sand shooting, respectively, surface treatment samples, are depicted. Failure stress is clearly decreasing with increasing strain rates. Besides, there is almost no influence of the overlap length. Results from both surface treatments are superimposed in Fig. 10. The sand shot samples have slightly higher failure strain.

4. Failure shear stress (shear strength)

Similarly to the failure strain, Figs. 11(a) and (b) show the sensitivity of the failure stress to the strain rate, obtained with different overlap lengths. It comes that the overlap length has almost no influence on the corrected failure stress. Results from both surface treatments are superimposed in Fig. 12. The failure stress increases when the strain rate increases up to a critical value and then drops sharply. The tendency is the same for both surface treatments.

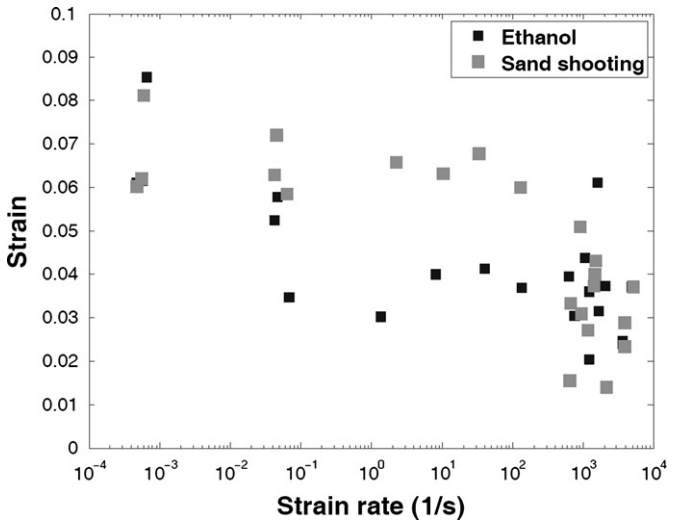

Fig. 12. Comparison between ethanol and sand shooting effects on the adhesive joint shear strength.

5. Discussion

In this study a large experimental program is undertaken to investigate the sensitivity of the mechanical behavior of a double-lap joints to strain rates ranging from $10^{-4}\,s^{-1}$ to $10^{4}\,s^{-1}$. To the best of the authors knowledge, no one has investigated such a wide range of strain rates before.

Three overlap lengths were considered in this study. Almost no influence of this parameter is observed on the failure strain and stress, which is a direct result of the use of correction coefficients proposed in Ref. [21]. Consequently, the use of these coefficients, which take the sample geometry into account, is relevant. Another methodology to deal with heterogeneous stress and strain fields would be to apply inverse techniques [33,34] or non-parametric methods [35,36].

Actually, the changes in the overlap length leads to a change in the coefficient λ, defined in Ref. [21], by almost 34%, which yields in a change of χ_ε and χ_σ of about 4% and a change in β_ε of about 38%. Therefore, it is hard to conclude that the joint strength is independent of the overlap length as we do not succeed to explore a wide range of χ_σ. However, we can conclude that the strain at failure is not influenced by the overlap length as we succeeded to vary β_ε of about 38%.

For the two considered types of surface treatments, the general tendency of the failure strain is a decrease whilst the strain rate increases for the three overlap length values. On the other hand, the shear strength increases with increasing strain rate till a critical value, which is about $10^{3}\,s^{-1}$, then it sharply decreases thereafter. The shear strength at quasi-static strain rates is about 60 MPa. It reaches about 120 MPa at the critical strain rate. Subsequently, it drops to approximately the quasi-static value. A possible onset of this drop at very high strain rates is adiabatic heat. A change of the failure mode can also explain this phenomenon. The failure strain and stress are of the same order for both surface treatments; however, the sand shooting values are slightly higher than obtained with ethanol surface treatment.

6. Conclusion

A detailed experimental study for adhesive joint failure strain and shear strength measurement has been presented. For this purpose, double-lap joint samples were tested on a wide range of strain rates considering two surface preparation treatments and three overlap lengths. Three different setups (five configurations) were used to explore strain rates ranging from $10^{-4}\,s^{-1}$ to $10^{4}\,s^{-1}$. Correction coefficients proposed in Ref. [21], were also used to take into account the sample geometry. For both substrates surface treatments and the three overlap lengths, it is found that bonded assemblies are highly strain rate sensitive. The failure strain decreases with increasing strain rate. Sand shooting effect provides slightly higher strain values than ethanol. Owing to the use of the correction coefficients, neither the shear strength nor the failure strain do depend on the overlap length.

References

[1] Zachary LW, Burger CP. Exp Mech 1980;20:162–6.
[2] Rossamanith HP, Shukla A. Ing Arch 1981;51:275–85.
[3] Beevers A, Ellis MD. Int J Adhes Adhes 1984;4:13–6.
[4] Jordan M. Int J Adhes Adhes 1988;8:36–46.
[5] Bezemer AA, Guyt CB, Vlot A. Int J Adhes Adhes 1998;18:225–60.
[6] Harris JA, Adams RD. Proc Inst Mech Eng C2 1985;199:121–31.
[7] Adams RD, Harris JA. Int J Adhes Adhes 1996;16:61–71.
[8] Satoh T, Miyazaki Y, Suzukawa Y, Nakazato N. JSAE Rev 1996;17:165–78.
[9] Goglio L, Rossetto M. Int J Impact Eng 2008;35:635–43.
[10] Keisler C, Lataillade JL. J Adhes Sci Technol 1995;9:395–411.
[11] Yokoyama T. Key Eng Mater 1998;145–149:317–22.
[12] Srivastava V, Shukla A, Parameswaran V. J Test Eval 2000;28:438–42.
[13] Adamvalli M, Parameswaran V. Int J Adhes Adhes 2008;28:321–7.

[14] Challita G, Othman R, Guégan P, Khalil K, Poitou A. Int J Mod Phys B 2008;22: 1081–6.
[15] Challita G, Othman R, Lebrun JM, Casari P, Guégan P. Proc DYMAT 2008:275–80, doi:10.1051/dymat/2009038.
[16] Yokoyama T. J Strain Anal Eng Des 2003;38:233–45.
[17] Chen X, Li Y. J Adhes Sci Technol 2010;24:291–304.
[18] Yokoyama T, Nakai K. J Phys IV 2006;134:789–95.
[19] Lawrence Wu CM, Li RKY, Yeung NH. J Electron Packaging Trans ASME 2003;125:93–7.
[20] Sato C, Ikegami K. J Adhes 1999;70:57–73.
[21] Challita G, Othman R. Int J Adhes Adhes 2010:236–44.
[22] Othman R, Guégan P, Challita G, Pasco F, LeBreton D. Int J Impact Eng 2009; 36:460–7.
[23] Othman R, Bussac MN, Collet P, Gary G. C R Acad Sci Sér IIb 2001;329: 369–76.
[24] Bussac MN, Collet P, Gary G, Othman R. J Mech Phys Solids 2002;50:321–49.
[25] Othman R, Bussac MN, Collet P, Gary G. J Phys IV 2003;110:397–404.
[26] Othman R, Gary G. Exp Mech 2007;47:295–9.
[27] Kolsky H. Proc Phys Soc B 1949;62:676–700.
[28] Krafft JM, Sullivan AM, Tipper CF. Proc R Soc Lond A 1954;221:114–27.
[29] Pope PH, Field JE. J Phys E Sci Instrum 1984:817–20.
[30] Zhao H, Abdennadher S, Othman R. Int J Impact Eng 2006;32:1174–89.
[31] Gary G, Degreff V. DAVID user manuel. Ecole Polytechnique, Plaiseau, France.
[32] Othman R, Blanc RH, Bussac MN, Collet P, Gary G. C R Mécanique 2002;320: 849–55.
[33] Kajberg J, Lindvist G. Int J Solids Struct 2004;41:3439–59.
[34] Kajberg J, Wikman B. Int J Solids Struct 2007;44:145–64.
[35] Aloui S, Othman R, Guégan P, Poitou A, El Borgi S. Mech Res Commun 2008;35:392–7.
[36] Othman R, Aloui S, Poitou A. Polym Test 2010;29:616–23.